JOURNAL OF Materials CHEMISTRY

Synthesis of Fe_3O_4 nanoparticles from emulsions

Z. H. Zhou,[a] J. Wang,*[a] X. Liu[a] and H. S. O. Chan[b]

[a]*Department of Materials Science, Faculty of Science, National University of Singapore, 119260, Singapore. E-mail: maswangj@nus.edu.sg*
[b]*Department of Chemistry, Faculty of Science, National University of Singapore, 119260, Singapore*

Received 22nd January 2001, Accepted 23rd February 2001
First published as an Advance Article on the web 10th April 2001

A unique oil-in-water emulsion route has been devised to synthesize nanosized magnetite (Fe_3O_4) particles using a small amount of cyclohexane as the oil phase, NP5 + NP9 as the surfactant phase, and a Fe(II)/Fe(III) salt solution as the aqueous phase. The Fe_3O_4 powder thus derived from the emulsion containing 88 wt% 0.3 M $FeSO_4 + Fe(NO_3)_3$ in the aqueous phase possesses an equiaxial morphology and an average particle size of <10 nm. Studies on the electrical conductivity of the emulsions as a function of Fe^{2+}/Fe^{3+} concentration in the aqueous phase revealed the complexation effect of the NP5 + NP9 surfactant towards Fe^{2+}/Fe^{3+} ions. The resulting particle size and morphology are therefore dependent on the amounts of surfactant and aqueous phase in the emulsion. A strongly alkaline aqueous phase favors the formation of Fe_3O_4, while a low alkalinity favors the formation of α-FeOOH. Magnetic property measurements and Mössbauer spectroscopic studies indicate that the emulsion-derived iron oxide powder is superparamagnetic, which becomes ferrimagnetic with decreasing measurement temperature.

I. Introduction

Nowadays functional nanoparticles are of industrial and scientific importance.[1] The rapid development of advanced electronics and microelectronic technologies requires continuous reduction in the size of the components employed, which in turn stimulates demand for the synthesis of ultrafine particles and functional materials. This lies in the fact that the properties of nanosized functional particles are very different from those of bulk materials of the same composition.[2,3] Research on many of these new properties and phenomena due to the refinement in particle sizes will lead to a better understanding of the relationships between structure and properties in many of these nanostructured materials. As an example, the development and realization of high density recording necessitates a significant refinement in the crystallite size of the recording media, which in turn requires a fundamental understanding of the magnetic behavior of nanophase materials.[4–6]

Various chemistry-based processing routes have been developed to synthesize several types of nanosized magnetic particles. For example, a microemulsion route was employed for the preparation of nanosized oxide particles.[6–8] Magnetic fluid containing magnetite particles of <10 nm in size were recently synthesized *via* a similar processing route.[7] Vollath and Szabo[9] reported a microwave plasma synthesis technique for maghemite powders with particle sizes below 10 nm using $FeCl_3$ and $Fe_3(CO)_{12}$ as the starting materials. There are also several other technologically promising techniques, including sol–gel, freeze-drying, laser pyrolysis and vaporization condensation.[1,10–12] However, one of the main challenges faced by almost all of these novel techniques is the ability to deliver well-dispersed nanoparticles with the desired compositional, structural and crystalline uniformity.

In this work, we explored the feasibility of synthesizing nanosized magnetite particles from oil-in-water emulsions, a technique which has recently been developed for the preparation of nanosized hydroxyapatite powders with improved crystallinity and morphology.[13] It offers the apparent advantages of a high production yield and usage of a very small amount of oil and surfactant phases, as compared to the water-in-oil microemulsions. In particular, the effects of various processing parameters, such as the pH value of the aqueous phase and the amount of surfactant phase, on the particle characteristics and magnetic properties of Fe_3O_4 powders derived from the emulsion are investigated.

II. Experimental

1. Materials

The starting chemicals used in this work were: iron sulfate ($FeSO_4 \cdot 7H_2O$) and iron nitrate ($Fe(NO_3)_3 \cdot 9H_2O$) of reagent grade (>99%, Fisher Scientific); ammonium hydroxide solution (28.0–30.0% NH_3, Ajax Chemicals, Australia) and sodium hydroxide (>99%, Sino Chemical Co. Pte. Ltd, Singapore); cyclohexane (reagent grade, Ajax Chemicals, Australia) and a mixed non-ionic surfactant consisting of polyoxyethylene(5) nonyl phenyl ether (NP5) and polyoxyethylene(9) nonyl phenyl ether (NP9) at a weight ratio of 1 : 1 (Albright and Wilson Asia Pte. Ltd., Singapore).

2. Experimental procedure

For comparison purposes, Fe_3O_4 powders were synthesized *via* two processing routes: conventional precipitation and precipitation in emulsion. Iron sulfate and iron nitrate were first dissolved in deionized water and then deoxygenated (by bubbling N_2 gas through the solution for half an hour) to make an aqueous solution containing Fe(III) and Fe(II) ions at a molar ratio of Fe(III)/Fe(II) = 2. In the conventional precipitation, the aqueous solution was added dropwise to a NaOH solution of pH = 13.5 with vigorous stirring. For the emulsion precipitation, emulsions of different compositions were prepared by mixing the aqueous solution with 9 wt% cyclohexane as the oil phase and various amounts of NP5 + NP9 as the surfactant. The emulsions containing aqueous NaOH phase as the water phase were also prepared using the same oil and surfactant phases. For aqueous phases of low pH, NH_4OH was used. The two types of emulsion were then mixed at an appropriate ratio while being continuously stirred. Additional

 DOI: 10.1039/b100758k

alkaline solution was added to bring the final alkalinity of the mixture to the desired pH value. The whole procedure was carried out in a glove-box filled with Ar of 99.9995% purity to prevent oxidation of the resulting Fe_3O_4. The resulting mixtures were then aged for 24 hours before being repeatedly washed with ethanol and water. The precursor particles were then retrieved by centrifugation and dried in a vacuum oven at 50 °C for 12 hours.

3. Characterization

Particle characteristics of the as-synthesized powders were studied using a transmission electron microscope (TEM, JEOL-100CX). A powder X-ray diffractometer (Cu-Kα, Phillips PW1729 X-ray diffractometer) and a Raman spectrometer (Renishaw 2000 micro-Raman system) were employed for phase identification. The specific surface areas were measured using a Brunauer–Emmett–Teller (BET) specific surface area analyzer (Quantachrome, NOVA2000). Their magnetic properties were characterized using a vibrating sample magnetometer (VSM, 41719.7, Oxford Instruments). Differential scanning calorimetry (DSC) analyses were carried out in N_2 at a heating rate of 10 °C min^{-1} using a DuPont 2950 thermal analyzer.

III. Results and discussion

X-Ray diffraction patterns for the powders derived from the emulsion and conventional precipitation are shown in Figs. 1(a) and (b), respectively. The emulsion employed for precipitation consisted of 9 wt% cyclohexane, 3 wt% NP5 + NP9 and an 88 wt% 0.3 M $FeSO_4 + Fe(NO_3)_3$ aqueous phase. Both precipitations were carried out under strongly alkaline conditions. The resulting materials from both processes can be identified as Fe_3O_4, the nanocrystalline nature of which is indicated by the much broadened appearance of the X-ray diffraction trace. Using Scherrer's equation for the FWHM of these diffraction traces, the crystallite sizes derived from emulsion and conventional precipitation were calculated to be 8.6 and 9.9 nm, respectively. To further confirm the formation of the Fe_3O_4 phase, Fig. 2 shows the Raman spectrum for the powder derived from the emulsion consisting of 9 wt% cyclohexane, 3 wt% NP5 + NP9 and an 88 wt% 0.3 M $FeSO_4 + Fe(NO_3)_3$ aqueous phase. The Raman peaks at 300, 530 and 660 cm^{-1} are indicative of Fe_3O_4.[14] No other iron oxide phases, such as α-Fe_2O_3 and γ-Fe_2O_3, are observed. The broadened Raman peaks suggest the nanocrystalline nature of Fe_3O_4 as indicated by the XRD trace in Fig. 1.

Figs. 3(a) and (b) are two bright field TEM micrographs,

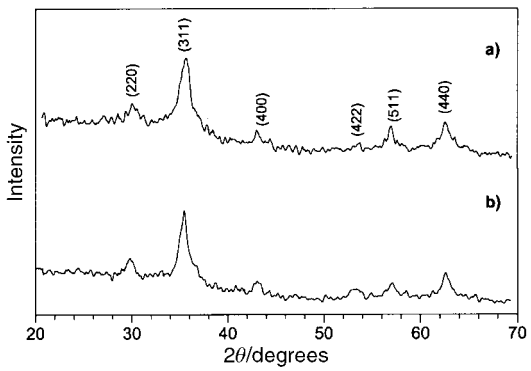

Fig. 1 XRD pattern for the powders derived from a) an emulsion consisting of 9 wt% cyclohexane, 3 wt% NP5 + NP9 and an 88 wt% 0.3 M $FeSO_4 + Fe(NO_3)_3$ aqueous phase and b) conventional precipitation in the aqueous phase.

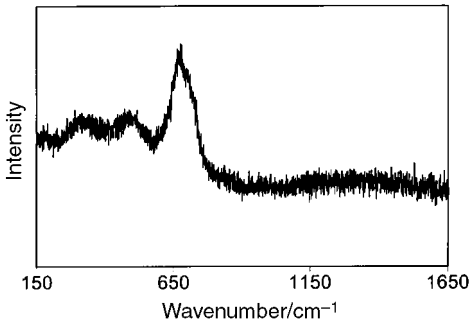

Fig. 2 Raman spectrum of the powder derived from an emulsion containing 9 wt% cyclohexane, 3 wt% NP5 + NP9 and an 88 wt% 0.3 M $FeSO_4 + Fe(NO_3)_3$ aqueous phase.

together with the associated SAD patterns for the above two powders, respectively. The Fe_3O_4 powder derived from conventional precipitation appears irregular in morphology and size, ranging from several nanometers to tens of nanometers. The associated SAD pattern indicates a poor uniformity in the crystallite size of the Fe_3O_4 particles. In contrast, the powder derived from the oil-in-water emulsion possesses a rather uniform particle morphology with an average particle size of <10 nm. These particles exhibit a more or less equiaxial morphology. The clear and well-defined diffraction rings in the SAD pattern reveal nanocrystallinity of rather uniform crystallite size.

The irregular particle size and morphology of the Fe_3O_4 particles derived from the conventional precipitation is associated with the fact that the nucleation and subsequent growth of Fe_3O_4 particles took place in an uncontrolled manner in the bulk aqueous phase. In the emulsion, by contrast, nanodomains of oil phase are dispersed in a continuous aqueous phase with the surfactant molecules residing at the interface. The formation of certain ceramic phases in such an emulsion system has been observed to relate to the complexation between cations and the surfactant molecules.[13] The complexation led to the nucleation and subsequent growth of a nanocrystalline ceramic phase in a controlled manner, resulting in an improvement in the uniformity of crystallite size and morphology. In particular, the complexation effect can lead to a significant increase in the crystallinity of ceramic phases, which are stable against further calcination at elevated temperatures. The small amount of surfactant therefore plays a critical role in modifying the particle and crystallite characteristics.

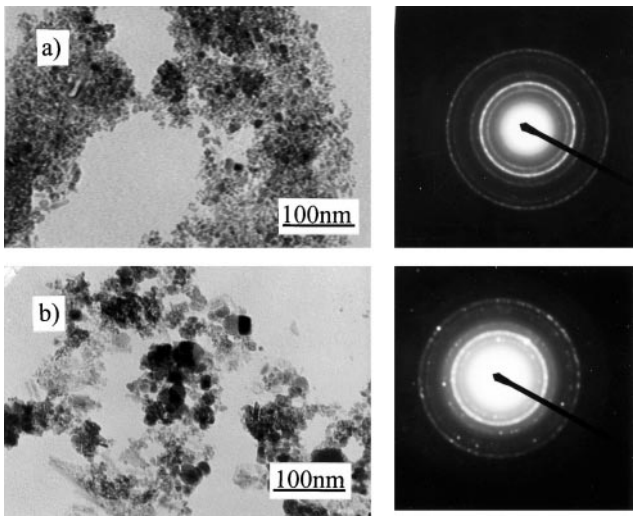

Fig. 3 TEM micrographs and the associated selected area diffraction (SAD) patterns for the powders derived from a) emulsion and b) conventional precipitation.

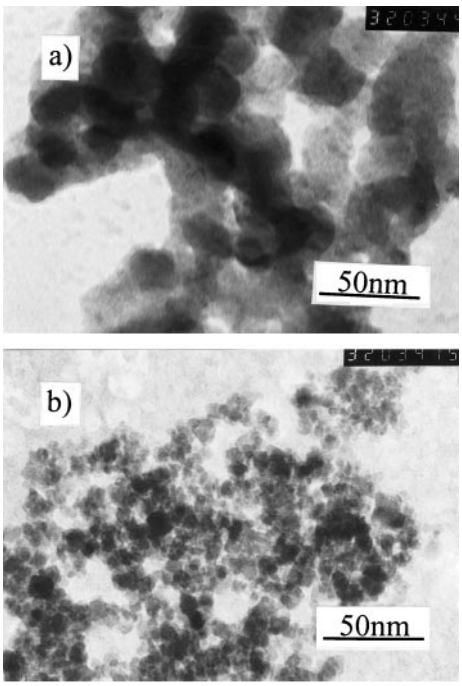

Fig. 4 TEM micrographs for the powders synthesized in emulsions containing a) 1.5 wt% and b) 3.0 wt% surfactant.

To investigate the effects of the amount of the surfactant phase in the emulsion on the particle and crystallite characteristics, Fe_3O_4 powders were synthesized in emulsions containing varying amounts of NP5 + NP9. As shown in Fig. 4, the Fe_3O_4 particles derived from the emulsion containing 1.5 wt% NP5 + NP9 were in the range of 20–30 nm, which is much coarser than those (< 10 nm) derived from the emulsion containing 3 wt% NP5 + NP9. This is further supported by the results of specific surface area analysis. For example, the powders derived from the emulsions containing 1.5 and 3.0 wt% NP5 + NP9 exhibit specific surface areas of 80.97 and 169.69 $m^2\ g^{-1}$, respectively. To gain a better understanding of the formation mechanism of the Fe_3O_4 particles in these emulsions, the dependence of electrical conductivity on cation (Fe^{2+}/Fe^{3+}) concentrations is plotted in Fig. 5, for the emulsions containing 1.5 and 3.0 wt% NP5 + NP9, respectively. At 3.0 wt% NP5 + NP9, the conductivity does not show any obvious change with increasing cation concentration up to 0.075 M, after which there is a sudden increase in the conductivity with further increases in cation concentration. This agrees with what is expected from the complexation effect of surfactant towards Fe^{2+}/Fe^{3+}. In the emulsions with a low cation concentration in the aqueous phase, most of the cations were trapped on the surface of cyclohexane droplets, where the surfactant molecules are aligned. Therefore, an increase in the

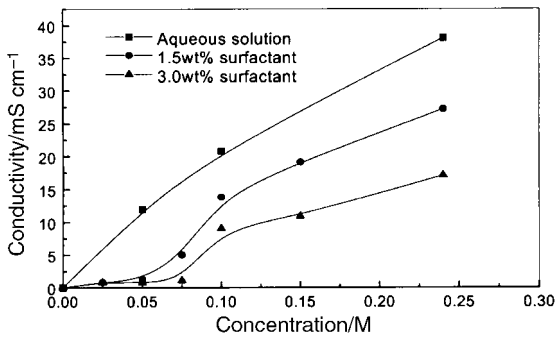

Fig. 5 The electrical conductivity of the emulsion as a function of $FeSO_4/Fe(NO_3)_3$ concentration in the aqueous phase and at a surfactant content of 1.5 and 3.0 wt%.

Fe^{2+}/Fe^{3+} concentration does not have much effect on the conductivity. With a steady increase in the cation concentration, Fe^{2+}/Fe^{3+} ions trapped at the oil droplet surface reach a saturation state, leaving the excess Fe^{2+}/Fe^{3+} in the aqueous phase of the emulsion where they are responsible for the sudden increase in conductivity. As shown in Fig. 5, a similar observation can be made for the emulsion containing 1.5 wt% NP5 + NP9, although the sudden rise in electrical conductivity occurs at a slightly lower Fe^{2+}/Fe^{3+} ion concentration (~0.05 M) than that in the emulsion containing 3.0 wt% NP5 + NP9. This can be easily explained by the fewer surfactant molecules in the former. For comparison purposes, the electrical conductivity of the aqueous solution containing Fe^{2+}/Fe^{3+} but no surfactant is also shown in Fig. 5. In this case the conductivity increases with the ion concentration in a more or less linear manner.

To study the effects of pH of the aqueous phase in the emulsion on the resulting particle and crystallite characteristics, the pH of the aqueous phase was varied in the range 8.5 to 13.5. This had a dramatic effect on the particle morphologies when examined using TEM. Figs. 6(a–c) are bright field TEM micrographs for the powders derived from the emulsions of the aqueous phase at pH 13.5, 10.5 and 8.5, respectively. Under strongly alkaline conditions (*i.e.*, pH = 13.5), the resulting particles exhibit a more or less equiaxial particle morphology and particle size of < 10 nm. In contrast, those particles derived from the composition of low pH (8.5) appear needlelike in morphology with the length varying from 20 to 80 nm and thickness from 3 to 8 nm. The emulsion containing an aqueous phase of intermediate pH (*i.e.* pH = 10.5) yielded a mixture of the equiaxial particles and needlelike rods.

The phases present in the three powders derived from the

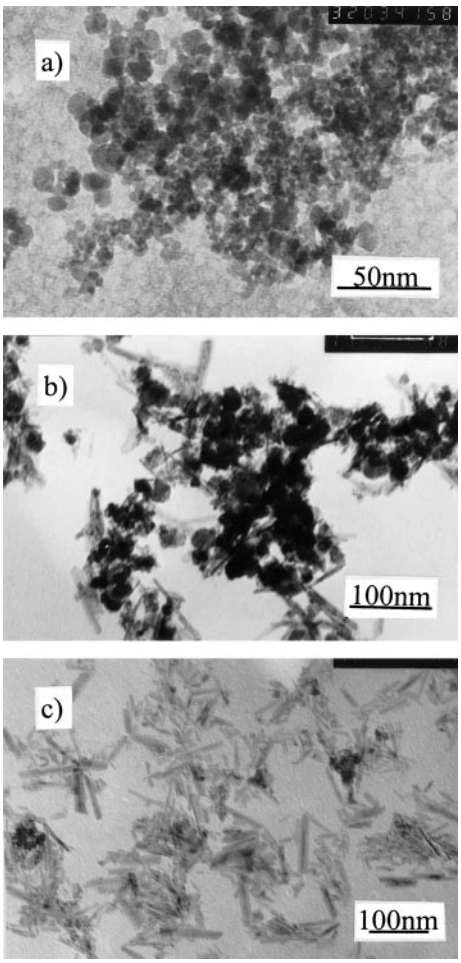

Fig. 6 TEM micrographs for the powders synthesized in emulsions of different pH values: a) pH = 13.5, b) pH = 10.5, c) pH = 8.5.

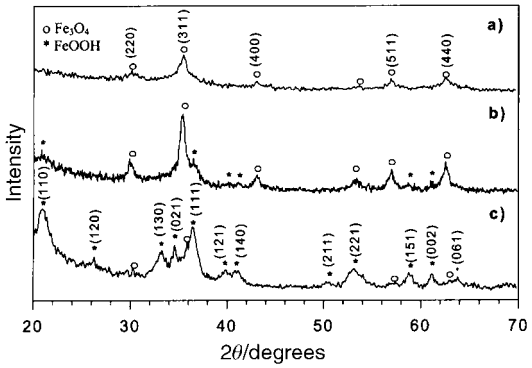

Fig. 7 XRD pattern for the powders formed at a) pH = 13.5, b) pH = 10.5, c) pH = 8.5 from the emulsions consisting of 9 wt% cyclohexane, 3 wt% NP5 + NP9 and an 88 wt% 0.3 M $FeSO_4$ + $Fe(NO_3)_3$ aqueous phase.

emulsions of pH 13.5, 10.5 and 8.5 were analyzed using X-ray diffraction (XRD). As shown in Figs. 7(a–c), all three powders demonstrate broadened XRD traces, suggesting that they consist of nanocrystallites. The peaks observed in Fig. 7(a) for the powder derived from the emulsion of pH 13.5 can all be assigned to Fe_3O_4. For the powder derived from the emulsion of pH 10.5, in contrast, the several small peaks located at 2θ angles of 21.2, 33.2, 39.9, 41.2, 59.0 and 61.4° suggest the occurrence of α-FeOOH in addition to the predominant Fe_3O_4 phase. These FeOOH peaks become more pronounced in the powder derived from the emulsion of pH 8.5, implying that α-FeOOH has become the predominant phase. Indeed, the diffraction peaks of Fe_3O_4, such as those of (311), (440), (511) and (220), can hardly be resolved due to the overlap with those of α-FeOOH, suggesting that the amount of Fe_3O_4 phase is minimized in the powder derived at low pH. By correlating these phase analysis results, it can be concluded that the equiaxial particles observed using TEM in Fig. 6 are Fe_3O_4, while the needlelike particles are α-FeOOH. It is also of interest to note that the peaks corresponding to Fe_3O_4 in Fig. 7(b) are sharper than those in Fig. 7(a). Calculation from FWHM data using Scherrer's equation gave a crystallite size of 30.7 nm for the powder derived from a pH 10.5 emulsion, compared to <9 nm for the powder derived from the pH 13.5 emulsion.

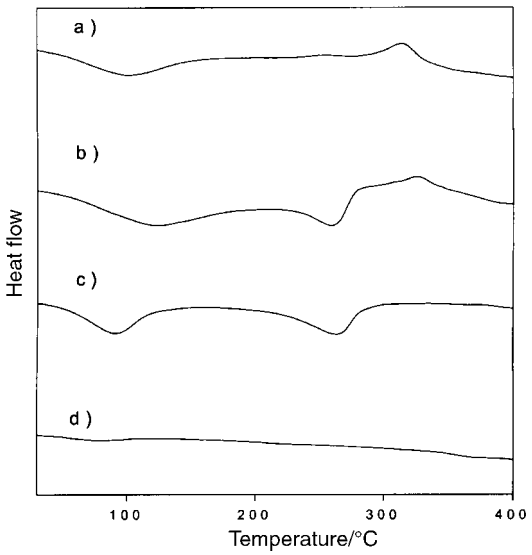

Fig. 8 DSC traces for the powders derived from emulsions consisting of 9 wt% cyclohexane, 3 wt% NP5 + NP9 and an 88 wt% 0.3 M $FeSO_4$ + $Fe(NO_3)_3$ aqueous phase of: a) pH = 13.5, b) pH = 10.5, c) pH = 8.5, respectively. d) DSC trace for the powder formed at pH = 13.5 and calcined at 400 °C for 1 hour.

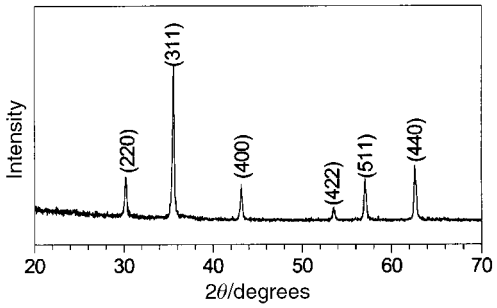

Fig. 9 XRD pattern for the powder formed at pH = 13.5 and calcined at 400 °C for 1 hour.

The above phase identification is further supported by the results of DSC thermal analysis. Fig. 8 plots the DSC traces for the powders derived from the emulsions of pH 13.5, 10.5 and 8.5, respectively. An endothermic peak is observed at around 100 °C for all three powders. This is due to the elimination of physically absorbed water and moisture. Further increases in temperature result in the emergence of an exothermic peak at 320 °C for the powder formed at pH 13.5 (Fig. 8(a)) and an endothermic peak at around 250 °C for the powder formed at pH 8.5 (Fig. 8(c)). The exothermic peak in the former is attributed to the crystal growth of Fe_3O_4 crystallites. To verify this, the powder was heated to 400 °C in N_2, followed by thermal analysis using DSC. No apparent exothermic reaction was observed at around 250 °C. Phase analysis using XRD also confirmed the establishment of a highly crystalline Fe_3O_4 phase after the calcination, as shown in Fig. 9. The occurrence of the endothermic peak at around 250 °C for the powder formed at pH 8.5 is related to the decomposition of FeOOH into oxide. As expected, both the endothermic and exothermic peaks occur for the powder formed at pH 10.5. As discussed above, the powder is a mixture of FeOOH and Fe_3O_4.

Based on the above phase and thermal analyses, it is apparent that an increase in the alkalinity of the aqueous phase in the emulsion favors the formation of Fe_3O_4. This agrees with the results of Wan *et al.*,[15] who observed the formation of iron oxide particles in a polymer matrix on lowering the acidity. The formation of Fe_3O_4 is therefore considered to proceed *via* the following three steps:

$$Fe^{2+}/Fe^{3+} + OH^- \rightarrow Fe(OH)_2/Fe(OH)_3$$

$$Fe(OH)_2/Fe(OH)_3 \rightarrow FeOOH \quad \text{(at low pH)}$$

$$FeOOH + Fe^{2+} \rightarrow Fe_3O_4 + H^+ \quad \text{(at high pH)}$$

Magnetic properties were measured at room temperature for the three powders derived from the emulsions of pH 8.5, 10.5 and 13.5, respectively. As shown in Fig. 10, the powders derived from pH 8.5 and pH 10.5 emulsions both exhibit a small hysteresis loop with a saturation magnetization of 4 and

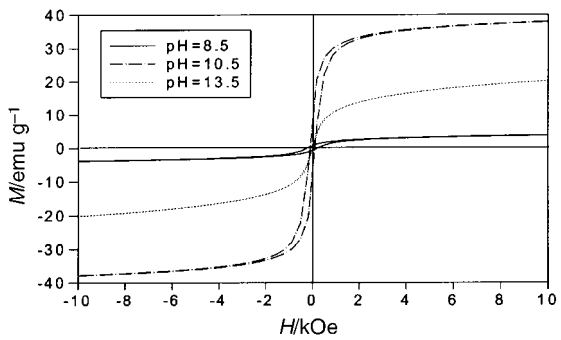

Fig. 10 Magnetization curves for the powders formed at different pH values when tested at room temperature.

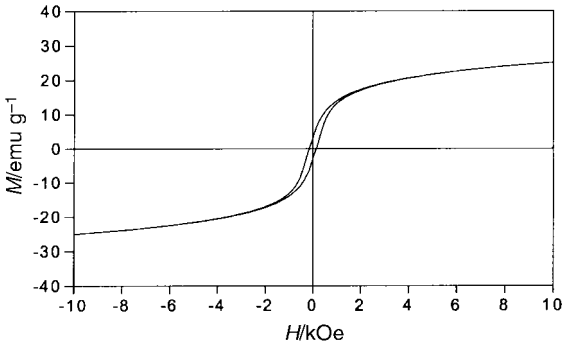

Fig. 11 Magnetization curve for the powder formed at pH = 13.5 when measured at 78 K.

38 emu g^{-1}, respectively. In contrast, the powder derived from the pH 13.5 emulsion demonstrates a typical superparamagnetic behavior, with zero coercivity and remanence. This is related to the fine crystallite sizes of Fe_3O_4 particles which are in the nanometer range. The material exhibits a saturation magnetization of $\sim$20 emu g^{-1}, which is far below that of bulk Fe_3O_4. As shown in Fig. 11, when measured at 78 K, it demonstrates a well established hysteresis loop, due to the magnetic blocking of fine Fe_3O_4 particles. Accordingly, its saturation magnetization is raised by 33%, with respect to that at room temperature. The magnetic behavior of nanocrystalline Fe_3O_4 is very sensitive to the crystallite and particle sizes.[2,3] The powder derived from the emulsion of pH 10.5 exhibits a higher saturation magnetization, although it contains a slightly smaller amount of Fe_3O_4 as compared to that in the powder derived from pH 13.5. This can be accounted for by the effects of crystallite size. As discussed above, those Fe_3O_4 particles formed at pH 10.5 were coarser in particle and crystallite sizes ($\sim$30 nm) than those of the powder formed at pH 13.5 ($<$10 nm). Superparamagnetic behavior is often observed at room temperature with iron oxide particles of $<$10 nm.[16] Coarser crystallites exhibit much higher saturation magnetization than finer ones. On the basis of phase analysis by XRD, the powder formed at pH 10.5 contained $\sim$15 wt% FeOOH. Therefore, the effects of FeOOH on the saturation magnetization in the powder can easily be compensated for by the size effect, as compared to that in the powder derived from pH 13.5, although the effects of other parameters can not be completely ruled out. For instance, due to the larger specific surface area in association with the finer particle sizes, the latter can be more "contaminated" by the surfactant, which may not be totally removed by washing. This can have a negative effect on the saturation magnetization of ultrafine particles derived from pH 13.5 emulsions.

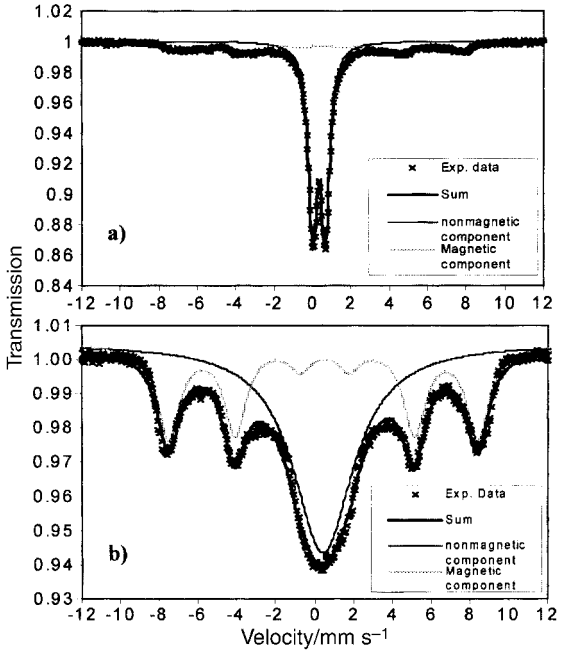

Fig. 12 ^{57}Fe Mössbauer spectrum of the powder formed at pH = 13.5 when measured at a) room temperature and b) 78 K.

The difference in magnetic properties between room temperature and 78 K for the nanocrystalline Fe_3O_4 particles derived from the emulsion of pH 13.5 is also supported by Mössbauer spectroscopic studies. Fig. 12(a) is the Mössbauer spectrum for the Fe_3O_4 powder derived from the emulsion consisting of 9 wt% cyclohexane, 3 wt% NP5 + NP9 and an 88 wt% 0.3 M $FeSO_4 + Fe(NO_3)_3$ aqueous phase when measured at room temperature. It consists of two significantly different components: a dominant central component and a small magnetic six-line component, indicating that the powder is superparamagnetic. The non-magnetic central component corresponds to superparamagnetic Fe_3O_4 particles, which constitute the majority phase. The magnetic component relates to the magnetic blocking of Fe_3O_4 nanoparticles. Such a broad six-line pattern is a result of overlapping between lines corresponding to Fe atoms in tetrahedral (A) and octahedral (B) sites due to the ultrafine crystallite sizes.[17,18] The spectrum at 78 K in Fig. 12(b) demonstrates a superparamagnetic to ferrimagnetic transition. At this low temperature, the magnetic six-line component becomes much more evident. The magnetically split component is attributed to $\sim$42% of the phase composition, indicating that some of the very fine Fe_3O_4 particles remain superparamagnetic at 78 K.

IV. Conclusions

Precipitation reactions in oil-in-water emulsions containing a small amount of cyclohexane as the oil phase, NP5 + NP9 as the surfactant phase, and aqueous Fe(II)/Fe(III) salt solution as the water phase give rise to nanocrystalline Fe_3O_4 particles of $<$10 nm in size. They exhibit improved uniformity in crystallite and particle sizes as compared to those derived from the conventional aqueous phase precipitation process. The formation of a nanocrystalline Fe_3O_4 phase in the emulsion is related to the complexation of Fe^{2+}/Fe^{3+} by the surfactant molecules. The pH of the aqueous phase has a dramatic effect on the resulting particle and crystallite characteristics. A highly alkaline aqueous phase in the emulsion favors the formation of Fe_3O_4 while a low pH favors the formation of α-FeOOH. The emulsion-derived Fe_3O_4 powder is superparamagnetic at room temperature due to its nanocrystalline nature and the refined particle sizes. There is a variation in magnetic properties between room temperature and 78 K for the nanocrystalline Fe_3O_4 particles, which is also shown by the Mössbauer spectroscopic studies.

References

1 M. P. Morales, S. Veintemillas-Verdaguer and C. J. Serna, *J. Mater. Res.*, 1999, **14**, 3066.
2 I. Bica, *Mater. Sci. Eng. B*, 1999, **68**, 5.
3 M. A. Lopez-Quintela and J. Rivas, *J. Colloid Interface Sci.*, 1993, **158**, 446.
4 R. H. Kodama, *J. Magn. Magn. Mater.*, 1999, **200**, 359.
5 Y. S. Kang, S. Risbud, J. F. Rabolt and P. Stroeve, *Chem. Mater.*, 1996, **8**, 2209.
6 V. Pillao and D. O. Shah, *J. Magn. Magn. Mater.*, 1996, **163**, 243.
7 J. A. Lopez-Perez, M. A. Lopez-Quintela, J. Mira and J. Rivas, *IEEE Trans. Magn.*, 1997, **33**, 4359.
8 V. Pillai and D. O. Shah, in *Industrial applications of microemulsions*, ed. C. Solans and H. Kunieda, Marcel Dekker, New York, 1997.

9 D. Vollath and D. V. Szabo, *J. Mater. Res.*, 1997, **12**, 2175.
10 C. Cannas, C. Giorgio, A. Musinu, G. Piccaluga and S. Z. Giorgio, *Z. Naturforsch., Teil A*, 1999, **54**, 513.
11 S. Veintemillas-Verdaguer, M. P. Morales and C. Serna, *J. Mater. Lett.*, 1998, **35**, 227.
12 T. Tachiwaki, M. Suzuki, H. Okajima, S. Koizumi, S. T. Ito and A. Hiraki, *Appl. Surf. Sci.*, 1993, **70–71**, 751.
13 G. K. Lim, J. Wang, S. C. Ng and L. M. Gan, *Langmuir*, 1999, **15**, 7472.
14 D. L. A. de Faria, S. V. Silva and M. T. de Oliveira, *J. Raman Spectrosc.*, 1997, **28**, 873.
15 W. Wan, W. Zhou and J. Li, *Synth. Met.*, 1996, **78**, 27.
16 R. M. Cornell and U. Schwertmann, *The Iron Oxides*, VCH, Weinheim, Germany, 1996
17 A. F. Lehlooh and S. H. Mahmood, *J. Magn. Magn. Mater.*, 1995, **151**, 163.
18 C. B. Koch, J. Z. Jiang and S. Morup, *Nanostruct. Mater.*, 1999, **12**, 233.